Astronomy & Astrophysics manuscript no. Printerfinal
December 22, 2016
©ESO 2016

arXiv:1612.07027v1 [astro-ph.GA] 21 Dec 2016

Importance of tunneling in H-abstraction reactions by OH radicals

The case of CH_4 + OH studied through isotope-substituted analogs

T. Lamberts[1], G. Fedoseev[2⋆], J. Kästner[1], S. Ioppolo[3], and H. Linnartz[2]

[1] Institute for Theoretical Chemistry, University Stuttgart, Pfaffenwaldring 55, 70569 Stuttgart, Germany
[2] Sackler Laboratory for Astrophysics, Leiden Observatory, Leiden University, PO Box 9513, 2300 RA Leiden, the Netherlands
[3] School of Physical Sciences, The Open University, Walton Hall, Milton Keynes, MK7 6AA, UK

Received XX/XX/XXXX / Accepted XX/XX/XXXX

ABSTRACT

We present a combined experimental and theoretical study focussing on the quantum tunneling of atoms in the reaction between CH_4 and OH. The importance of this reaction pathway is derived by investigating isotope substituted analogs. Quantitative reaction rates needed for astrochemical models at low temperature are currently unavailable both in the solid state and in the gas phase. Here, we study tunneling effects upon hydrogen abstraction in CH_4 + OH by focusing on two reactions: CH_4 + OD $\longrightarrow$ CH_3 + HDO and CD_4 + OH $\longrightarrow$ CD_3 + HDO. The experimental study shows that the solid-state reaction rate R_{CH_4+OD} is higher than R_{CD_4+OH} at 15 K. Experimental results are accompanied by calculations of the corresponding unimolecular and bimolecular reaction rate constants using instanton theory taking into account surface effects. From the work presented here, the unimolecular reactions are particularly interesting as these provide insight into reactions following a Langmuir-Hinshelwood process. The resulting ratio of the rate constants shows that the H abstraction (k_{CH_4+OD}) is approximately ten times faster than D-abstraction (k_{CD_4+OH}) at 65 K. We conclude that tunneling is involved at low temperatures in the abstraction reactions studied here. The unimolecular rate constants can be used by the modeling community as a first approach to describe OH-mediated abstraction reactions in the solid phase. For this reason we provide fits of our calculated rate constants that allow the inclusion of these reactions in models in a straightforward fashion.

Key words. Astrochemistrty - Molecular processes - ISM:molecules - Methods:laboratory

1. Introduction

Radicals in ices are important players in solid-state interstellar chemistry (van Dishoeck et al. 2013; Öberg 2016). In particular, OH radicals seem to be abundant in ices (Chang & Herbst 2014; Lamberts et al. 2014); they play a role during solid-state water formation processes (Cuppen et al. 2010; Oba et al. 2012; Lamberts et al. 2013, 2016a), are involved in the formation of solid CO_2 (Oba et al. 2010; Noble et al. 2011; Ioppolo et al. 2013), and have been postulated to be crucial for the formation of complex organic molecules (Garrod 2013; Acharyya et al. 2015). Abstraction reactions of the type OH + HC−R $\longrightarrow$ H_2O + C−R may form carbon-based radicals that can subsequently react with one another forming molecules that contain C–C bonds. Such abstraction reactions have recently been studied experimentally in the gas phase and show the importance of tunneling (Shannon et al. 2013; Caravan et al. 2015). In the solid state abstraction reactions along the hydrogenation line, CO−H_2CO−CH_3OH was shown to provide extra pathways to form methylformate, ethylene glycol, and glycol aldehyde Chuang et al. (2016). Although these gas-phase and solid-state reactions have been implemented in some astrochemical models, this is not yet common practice; for comparison, we refer the reader to Garrod (2013) and Acharyya et al. (2015) to Vasyunin & Herbst (2013) and Furuya & Aikawa (2014), for example. Moreover, although a hydrogen transfer is involved, the role of tunneling at low temperature has not yet been investigated specifically. This is the main goal of the present work.

Tunneling can be defined as the quantum mechanical phenomenon that allows a particle to cross a barrier without having the energy required to surmount this barrier, that is, reaction routes that classically cannot occur at low temperatures become accessible. As a result of the mass dependence of tunneling processes, reactions with hydrogen, for instance, will be faster than with deuterium.

Although OH-mediated abstractions of hydrogen can occur with any hydrocarbon, the simplest example concerns CH_4. Interstellar methane is proposed to be a starting point of complex organic chemistry (Öberg 2016). It likely originates from carbon hydrogenation on the grain surface that occurs simultaneously with H_2O formation with abundances of ∼5% CH_4 with respect to H_2O (Lacy et al. 1991; Boogert et al. 1998; Öberg et al. 2008). H_2O ices are formed via hydrogenation of OH and therefore, OH will thus naturally be present in the ice (Lamberts et al. 2014). Furthermore, weak FUV irradiation has been shown to result in photodissociation of water, which also yields OH (Garrod 2013; Drozdovskaya et al. 2016). As mentioned above, hydroxyl radicals are known to react with CO and produce CO_2 that has been abundantly seen and modeled in the water-rich layers of the ice. Since methane is present in the same layer, reactions of methane with OH are therefore expected to take place as well. Note that these molecules have also recently been seen to co-exist in the coma of 67P/Churyumov-Gerasimenko (Bockelée-Morvan et al. 2016). Here, we perform a proof-of-concept study on the importance of tunneling for the reaction CH_4 + OH $\longrightarrow$ H_2O + CH_3,

⋆ Current address: INAF–Osservatorio Astrofisico di Catania, via Santa Sofia 78, 95123 Catania, Italy

both experimentally in the solid phase and through high-level calculations of reaction rate constants in the gas phase. The latter are performed in such a way that the results also allow us to draw conclusions on the solid state processes.

The experiments that are described in Section 2.1 make use of OH (or OD) produced in the solid phase. Calculations performed by Arasa et al. (2013); Meyer & Reuter (2014) show that dissipation of excess energy takes place on a picosecond timescale. Therefore, thermalized reactions with the produced hydroxyl radicals occur as would be the case in the interstellar medium (ISM). The gas-phase activation energy for hydrogen abstraction from CH_4 is reported to be ~3160 K = 26.3 kJ/mol without zero-point energy (ZPE) correction (Li & Guo 2015). For the reaction to proceed at cryogenic temperatures, tunneling needs to be efficient. To the best of our knowledge, rate constants below 200 K are not currently available, either in the gas phase or in the solid state (Atkinson 2003). Here, the role of tunneling is studied by comparing two sets of experiments, one probing H-abstraction – $CH_4 + OD \longrightarrow CH_3 + HDO$ – and another probing D-abstraction – $CD_4 + OH \longrightarrow CD_3 + HDO$. These surface reactions have already been studied experimentally (Wada et al. 2006; Hodyss et al. 2009; Weber et al. 2009; Zins et al. 2012). We extend on this previous work by quantitatively studying the isotope effect in the aforementioned abstraction reactions.

The calculations that are described in Section 2.2 incorporate tunneling through instanton theory, which allows reaction rate constants to be calculated at low temperatures. Also, previously published theoretical rate constants only reach down to 200 K, and, moreover, only bimolecular values were reported (Wang & Zhao 2012; Allen et al. 2013). In order to compare this with the present solid-state experiments, however, unimolecular rate constants are more relevant. These correspond to the decay rate of a pre-reactive complex of OH and CH_4 on the surface, that is, from a configuration where the species have met while being thermalized, as is the case in the Langmuir-Hinshelwood (LH) mechanism.

In Section 3 the experimental results and theoretical calculations are presented. The final Section discusses the astrophysical consequences. It is common for astrochemical models to make use of a rectangular barrier approximation in the description of tunneling; see Hasegawa et al. (1992), for example. We show here that kinetic isotope effects calculated while taking tunneling into account explicitly yield values that differ by several orders of magnitude with respect to instanton calculations. This work also ultimately shows that it is the combination of experiments, theory, and the method of implementation of results in models which is key to understanding the general behavior of tunneling in H-abstraction reactions by OH radicals.

2. Methodology

2.1. Experimental procedure

The experiments have been performed using the ultra-high vacuum (UHV) setup SURFRESIDE. All relevant experiments are listed in Table 1. Experimental details for the setup configuration used here are available from Ioppolo et al. (2008). Briefly, a gold-coated copper substrate is placed in the center of a stainless steel UHV chamber ($P_{\rm base,\,main} < 4 \times 10^{-10}$ mbar) and kept at a temperature of 15 K using a He closed-cycle cryostat. For all experiments, a CH_4:O_2 (CD_4:O_2) mixture is continuously deposited simultaneously with a D (H) beam. This is a so-called co-deposition experiment. Mixtures of CH_4 or CD_4 with O_2 are deposited at an angle of 45° with a deposition rate of 0.45 Langmuir per minute, controlled by a precise all-metal leak valve, where 1 Langmuir corresponds to ~1.3×10^{-6} mbar s^{-1}. Such an exposure rate corresponds to ~2.7×10^{12} molecules of CH_4 or CD_4 cm^{-2} s^{-1} and ~6.7×10^{11} molecules O_2 cm^{-2} s^{-1}. Gas mixture preparation is performed in a pre-pumped stainless steel dosing line ($P_{\rm base,\,dosing\,line} < 10^{-5}$ mbar) directly attached to the metal leak valve. A new mixture is prepared for each experiment. The hydroxyl radicals are produced in the ice via hydrogenation or deuteration of O_2, for example, $H + O_2 \longrightarrow HO_2$ ($D + O_2 \longrightarrow DO_2$) and $H + HO_2 \longrightarrow 2\,OH$ ($D + DO_2 \longrightarrow 2\,OD$) (Lamberts et al. 2014). This yields cold hydroxyl radicals via quick energy dissipation as explained above. Note that these hydroxyl radicals are thus formed during deposition, that is, methane molecules are in the direct vicinity of the formed OH radicals as a result of the 4:1 CH_4:O_2 ratio. The H or D atoms needed for this are generated in a thermal cracking source (Tschersich & von Bonin 1998) facing the substrate. H_2 or D_2 molecules are dissociated after collisions with the hot walls ($T \approx 2120$ K) of a tungsten capillary pipe, which in turn is surrounded by a heated tungsten filament. A nose-shaped quartz pipe along the beam path cools down the beam to roughly room temperature before it reaches the surface. The dissociation fraction mentioned by Tschersich (2000) is ~40% at 2120 K for a pressure higher than that used here, inferring a higher dissociation ratio for the present experiments. However, this should be considered to be an upper limit, since H-H recombination may take place on the walls of the quartz pipe as well as on the ice surface. From Ioppolo et al. (2010), we can infer a H_2/H ratio of approximately 10-15%. The H and D-fluxes used here are ~6×10^{13} and ~3×10^{13} atoms cm^{-2} s^{-1} (Ioppolo et al. 2010). This ensures an overabundance of at least an order of magnitude of H (D) atoms with respect to CD_4 (CH_4) and O_2 on the surface.

Table 1. List of performed co-deposition experiments (1 and 5) and control co-deposition experiments (2–4, 6,7).

No.	Ice mixture		Species	Duration (min)
1	$CH_4 : O_2$	4:1	D (+ D_2)	300
2	$CH_4 : O_2$	4:1	D_2	300
3	CH_4		D (+ D_2)	180
4	$CH_4 : N_2$	1:4	D (+ D_2)	300
5	$CD_4 : O_2$	4:1	H (+ H_2)	300
6	$CD_4 : O_2$	4:1	H_2	196
7	CD_4		H (+ H_2)	300

The ice composition is monitored using reflection absorption infrared spectroscopy (RAIRS) in the spectral range 700 – 4000 cm^{-1} (14 – 2.5 μm) with a spectral resolution of 0.5 cm^{-1} and averaging 512 spectra, using a Fourier transform infrared spectrometer. RAIR difference spectra are acquired with respect to a background spectrum of the bare gold substrate at 15 K.

Straight baseline segments are subtracted from all acquired spectra, using five reference points: 699, 1140, 1170, 1830, and 4000 cm^{-1}. All spectra shown are normalized to a duration of 300 min (see Table 1) to allow direct comparison in the figures below. Furthermore, for all spectra, three data points are binned to allow for some smoothing. The reproducibility of the experiments is warranted by a triple execution and reproduction of exp. 1. The resulting data of only one of these measurements is shown in Figs. 1 and 2.

Control experiments have been chosen to exclude reactions not involving OD (OH) and to exclude the direct abstraction of H (D) from CH_4 (CD_4) by D (H) atoms. Table 1 provides an

overview of the CH_4 + OD and CD_4 + OH experiments (exps. 1 and 5) and control experiments (exps. 2–4, 6, and 7). Control experiments 2 and 6 are directly related, since any products that are formed both in experiments 1 and 2 (or 5 and 6) are not caused by any reactions of the hydroxyl radical, because O_2 and D_2 (H_2) do not produce OD (OH). The control experiments 3, 4, and 7 aim to exclude the direct abstraction of H (D) from CH_4 (CD_4) by D (H) atoms. That is, if no abstraction products are detected in control experiments 3, 4, and 7, any differences that are seen between experiments 1 and 5 are due to reactions involving the hydroxyl radical only.

2.2. Computational details

To obtain reaction rate constants that take tunneling into account explicitly, we use instanton theory (Miller 1975; Callan & Coleman 1977). This is based on statistical Feynman path integrals that incorporate quantum tunneling effects, (see Kästner (2014); Richardson (2016)). The instanton is the optimal tunneling path, which is usually different from the minimal energy path between stationary points (reactant, transition, and product states). Instanton theory is applicable when the temperature is low enough for the path to spread out, or to put it differently, when tunneling dominates the reaction. This is typically the case below the crossover temperature, $T_C = \hbar\omega_b/2\pi k_B$, where ω_b is the absolute value of the imaginary frequency at the transition state.

Instanton theory as implemented in DL-FIND (Kästner et al. 2009; Rommel et al. 2011) is used in this study on the potential energy surface (PES) of Li & Guo (2015) which is fitted to CCSD(T)-F12/AVTZ data. The Feynman paths of the instantons are discretized to 200 images. Instanton geometries are converged until the gradient is below 10^{-9} atomic units.

The experimental data show that in the solid state, the reaction takes place between thermalized species (Section 3.1). These species have already approached one another through surface diffusion prior to reaction via the LH mechanism. The relevant rate constant calculated here describes the decay of this encounter complex. Therefore, we calculate unimolecular reaction rates excluding the probability of meeting, hence the unit of s^{-1}. The vibrational adiabatic barrier for this process, that is, originating from the Van der Waals complex in the reactant channel, is 2575 K (21.4 kJ/mol) on the PES while it is slightly higher, 2670 K (22.2 kJ/mol), when calculated directly with CCSD (T)-F12/VTZ-F12 on the PES geometries.

We model the surface by allowing for instant dissipation of energy through the constant temperature assumed in instanton calculations. Furthermore, the concentration of the reactants on a grain is higher than in the gas phase. We provide rate constants that are independent of the concentration, as this is dealt with separately in astrochemical models. However, our structural model includes only CH4 and OH and not explicit surface atoms. On the surface, rotational motions are restricted and therefore the rotational partition function is kept constant, that is, frozen-out. However, the rotational symmetry factor (Fernández-Ramos et al. 2007) of 3 between the C_{3v}-symmetric Van der Waals complex and the transition state or instanton is taken into account. Finally, another effect of the surface can be on the activation barrier of the reaction. This is neglected in our approach. In the experiment, the surface consists of CH_4, O_2, H_2O_2, and H_2O. Both CH_4 and O_2 do not pose strong restrictions on the reactants in terms of interaction or steric hindrance, while the main contribution to the ice comes from CH_4. Therefore, the only assumption we make is that the minority species H_2O and H_2O_2 do not impact strongly on the reaction.

Bimolecular rates related to the gas-phase mechanism are also calculated for comparison with gas-phase experiments, see Appendix A. There, the full rotational partition function including the rotational symmetry factor of 12 is taken into account and CH_4 and OH reactant state structures are used that are calculated with ChemShell (Metz et al. 2014) on a CCSD(T)-F12/VTZ-F12 level using Molpro 2012 (Werner et al. 2015).

Although OH has two degenerate spin states in the $^2\Pi$ ground state, when reacting with closed-shell molecules, both states are reactive and no additional correction factors for the rate constants are needed (Graff & Wagner 1990; Fu et al. 2010).

In order to provide input for astrochemical modelers, we fit a rate expression, Eqn. 1 (Zheng & Truhlar 2010), to the calculated rate constants;

$$k = \alpha \left(\frac{T}{300}\right)^{\beta} \exp\left(-\frac{\gamma(T + T_0)}{(T^2 + T_0^2)}\right). \quad (1)$$

This expression is more suitable for describing tunneling reactions than the commonly used Kooij expression. The parameters α, β, γ, and T_0 are all fitting parameters, where α has the units of the rate constant, β regulates the low-temperature behavior, and γ and T_0 can be related to the activation energy of the reaction. β is set to 1 since this results in the correct low-temperature behavior. Instanton rate calculations are used for the fits below the crossover temperature T_C, while rate constants obtained from transition state theory - including quantized vibrations and a symmetric Eckart model for the barrier - are used above T_C where tunneling plays a minor role.

As a final remark, it is important to keep the difference between the reaction rate, R, and the rate constant, k, in mind. Experimentally, only effective rates or the ratio of effective rates can

Table 2. Peaks identified in the difference spectrum between exps. 1 and 2, depicted in Fig. 1.

$\tilde{\nu}$	Specification			Species	Ref.
(cm^{-1})	[a]	[b]	[c]		
3434	w	b		HDO	1
3015	s	n		CH_4	2
2957	w			CH_3D	3
2904	m	n		CH_4	2
2817	m	n		CH_4	2
2718	w	b	u		
2620	w		p	CH_3D	3
2440	s	b		D_2O_2	1
2192	w			CH_3D	3
2115	m	b		D_2O_2	1
1530	w	b	p	CH_3D	3
1464	w	n		CH_3D	3
	w	b	p	HDO	1
1400	w	b	u		
1304	s	n		CH_4	2
1195	w	b	u		
1154	m	n		CH_3D	3
1020	s	b		D_2O_2	1
870	s	b		D_2O_2	4

[a] w = weak, m = medium, s = strong
[b] b = broad, n = narrow
[c] u = unidentified, p = possible

References. (1) Oba et al. (2014); (2) Edling et al. (1987); (3) Momose et al. (2004); (4) Giguère & Srinivasan (1975)

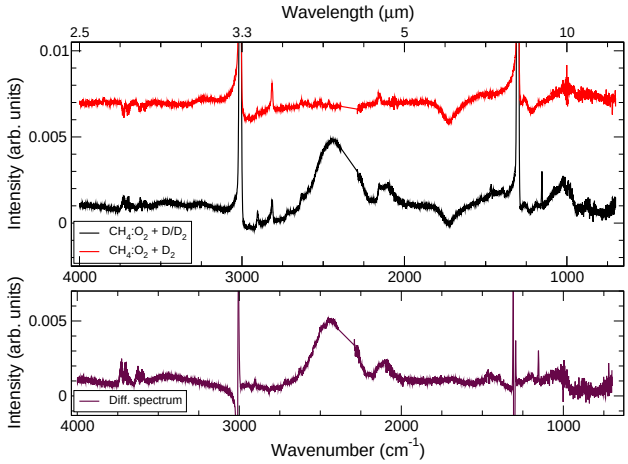

Fig. 1. Full RAIR spectrum of exps. 1 (black) and 2 (red) and their difference curve (purple). See Table 2 for the assignment of the peaks. Note that the CO_2 band has been removed for reasons of clarity.

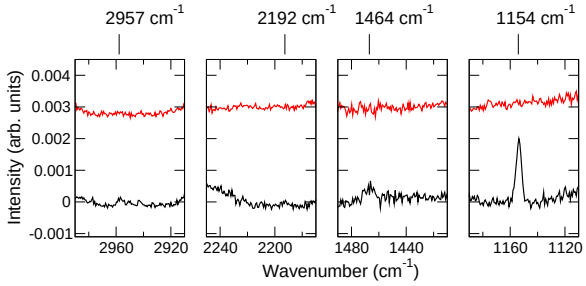

Fig. 2. RAIR spectrum of exps. 1 (black) and 2 (red), zoomed-in on the regions of interest of known CH_3D IR transitions. See Table 2 for the assignment of the peaks.

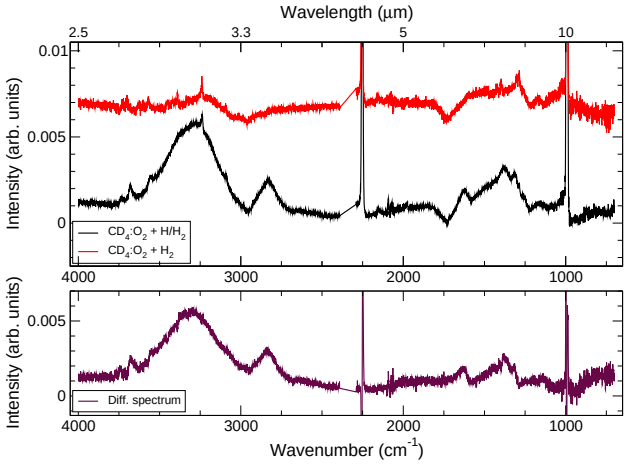

Fig. 3. Full RAIR spectrum of exps. 5 (black) and 6 (red) and their difference curve (purple). Note that the CO_2 band has been removed for reasons of clarity.

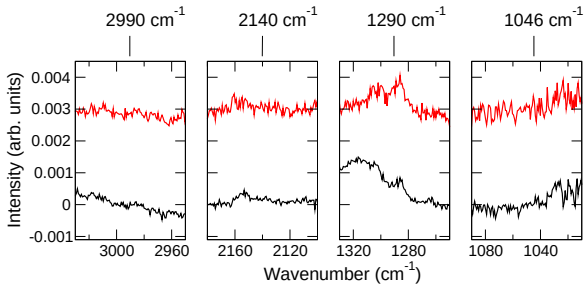

Fig. 4. RAIR spectrum of exps. 5 (black) and 6 (red), zoomed-in on the regions of interest of known CD_3H IR transitions.

be determined. This is because, experimentally, one can only detect the change in the production of a final product, meaning it is not possible to separate the diffusion and reaction processes. Theoretically, however, a rate constant that is related exclusively to the decay of the encounter complex can be calculated, that is, after the diffusion has already taken place. Therefore, the kinetic isotope effect (KIE) for H-abstraction vs. D-abstraction derived from the effective rate and derived from the rate constants do not necessarily need to be identical.

3. Results & discussion

3.1. Experimental – infrared spectra

Figures 1 and 2 depict the final RAIR spectra acquired for exps. 1 and 2 (upper panels). The difference spectrum between exps. 1 and 2 is also given (lower panels), either showing the full spectral window (Fig. 1) or zoomed-in on the regions of interest of CH_3D (Fig. 2). The same holds for exps. 5 and 6 (Fig. 3), and zoomed-in on the regions of interest of CD_3H (Fig. 4). In Table 2, the peak positions that can be determined in the difference spectrum between exps. 1 and 2 are listed with their corresponding assignment and reference.

The main outcome of the surface experiments is that at our detection level, abstraction from methane is only found to take place during exp. 1. The reactants available there, CH_4, O_2, and D, can undergo several reactions. The relevant ones are listed below.

$$O_2 + D \rightarrow DO_2 \quad \text{(R1)}$$
$$DO_2 + D \rightarrow 2\ OD \quad \text{(R2)}$$
$$2\ OD \rightarrow D_2O_2 \quad \text{(R3)}$$
$$D + D_2O_2 \rightarrow D_2O + OD \quad \text{(R4)}$$
$$CH_4 + OD \rightarrow CH_3 + HDO \quad \text{(R5)}$$
$$CH_3 + D \rightarrow CH_3D \quad \text{(R6)}$$
$$CH_3 + OD \rightarrow CH_3OD \quad \text{(R7)}$$
$$CH_3 + CH_3 \rightarrow C_2H_6 \quad \text{(R8)}$$

The equivalent reactions, but with deuterium substituted for hydrogen (starting from R1), are applicable for experiment 5. Note that the reaction $CH_4 + D \longrightarrow CH_3 + HD$ has been excluded from the list of possible reactions. This is explained below.

We clearly identify D_2O_2 and CH_3D infrared features and a weak stretching mode of HDO in Fig. 1; see Table 2 for the various peak positions. The bending mode of HDO at 1475 cm^{-1} is not clearly visible as a result of the signal-to-noise (S/N) level. The bending mode is at least four times weaker than the stretching mode, which is not detectable for the S/N ratio achieved here (Oba et al. 2014). This means that the produced OD radicals either form D_2O_2 or abstract an H-atom from CH_4. The availability of D atoms on the surface results in the barrierless deuteration of a CH_3 radical. Since the D atoms are abundant and diffuse quickly, other radical-radical reactions are prevented. The CH_3OD or C_2H_6 yields lie below the sensitivity of our RAIRS technique, that is, reactions R7 and R8 are not relevant here.

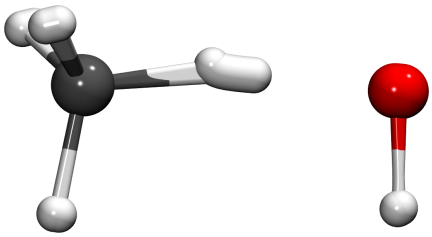

Fig. 5. Instanton path for CH_4 + OH at 200 K.

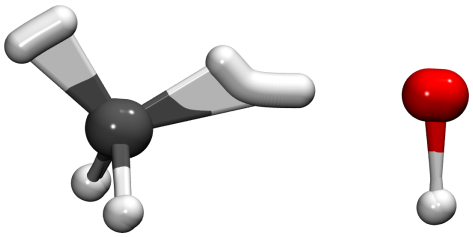

Fig. 6. Instanton path for CH_4 + OH at 100 K.

Note that the abstraction reaction between HO_2 and CH_4 has a barrier of > 10000 K (Aguilera-Iparraguirre et al. 2008), and we therefore exclude any CH_3 radical production via this route.

Furthermore, none of the control experiments (numbers 2-4) resulted in the detection of CH_3D. This means that the CH_3D detected in experiment 1 is not the cause of contamination (follows from experiment 2) nor the result of H-abstraction from CH_4 by D atoms directly (follows from control experiments 3 and 4). In other words, in our experimental setup, the reaction between CH_4 and the D atom does not proceed within our experimental sensitivity. Since the same setup is used for experiments 1, 3, and 4, essentially for identical conditions, we conclude that the reaction CH_4 + OD is more efficient and the only one responsible for the formation of the observed CH_3D. This result can be rationalized by realizing that the reaction $CH_4 + H \longrightarrow CH_3 + H_2$ has a high barrier of 6940-7545 K (Nyman et al. 2007; Corchado et al. 2009), making it highly unlikely to be competitive at the low temperatures considered here, even if it were to occur via tunneling. Indeed, the (bimolecular) rate constants calculated on several PES at 300 K are six orders of magnitude lower than the bimolecular rate constants calculated here for CH_4 + OH (compare Corchado et al. 2009, Espinosa-García et al. 2009, and Li et al. 2013 with values mentioned in Appendix A).

The next question is whether or not the isotope-substituted reaction R5, CD_4 + OH $\longrightarrow$ CD_3 + HDO leads to D-abstraction by OH radicals. In this case, the mass of the atom that is transferred is twice as high and if tunneling is important, the reaction rate should drop significantly. In Fig. 3, and especially from the zoomed-in spectra in Fig. 4, it is clear that no detectable amounts of CD_3H are produced during experiment 5. Since OH radicals are present, H_2O_2 is formed and can be seen at its respective peak positions, around 3315, 2835, and 1385 cm^{-1} (Oba et al. 2014). Furthermore, the OH radicals that are produced are not being used for reactions with CD_4 and therefore are available for other reactions, leading to the formation and detection of the H_2O bending mode at 1630 cm^{-1}, while the stretching mode overlaps with that of H_2O_2. H_2O can also be formed via $H + H_2O_2 \longrightarrow H_2O + OH$ in contrast to the formation of D_2O via $D + D_2O_2 \longrightarrow D_2O + OD$ as a result of the kinetic isotope effect (Lamberts et al. 2016b). The control experiments 6 and 7 do not result in the detection of any CD_3H either.

Since neither experiment 1 nor 5 results in breaking of the bond between the carbon atom and hydrogen or deuterium atom, we can be certain that the OD and OH radicals that are formed in the ice thermalize prior to attempting to react. We propose that the origin of the difference between experiments 1 and 5 is the tunneling of the H or D atom that is being transferred from the carbon atom to the oxygen atom. Experimentally, it is not trivial to quantify the ratio between the effective rates, but we can state that R_{CD_4+OH} is smaller than R_{CH_4+OD}. A further quantification is the aim of the following section, using theoretical calculations of rate constants.

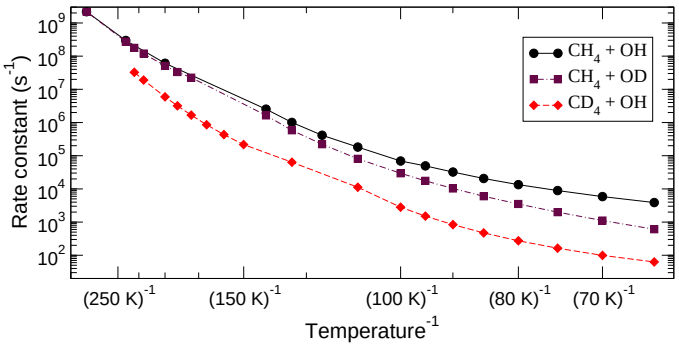

Fig. 7. Arrhenius plot of the unimolecular reaction rate constants for three isotopological analogs of reaction R5: CH_4 + OH (black, solid), CH_4 + OD (purple, dashed-dotted), and CD_4 + OH (red, dashed).

3.2. Theoretical – LH unimolecular rate constants

Rate constants are calculated using instanton theory. An instanton path essentially shows the delocalization of the atoms involved in the reaction. This deviates from the classical picture of overcoming a barrier and visualizes the tunneling through a barrier. More delocalization is seen at lower temperatures, where tunneling indeed plays a larger role. In Fig. 5 the instanton path is depicted for the reaction between CH_4 and OH at 200 K. This geometry corresponds to the geometry of the optimized transition state where the O–H bond is in an eclipsed configuration with one C–H bond. At low temperature, that geometry becomes unstable and the instanton switches to a staggered position. Fig. 6 gives the corresponding geometry at 100 K. This instability leads to a temperature region where instanton rates become unreliable (Meisner et al. 2011). In the current paper, we only give rate constants that do not lie within the switching regime. Therefore, not all rate constants can be calculated at exactly the same temperatures, as is visible in Table 3. Furthermore, rates can only be calculated down to a certain temperature (here, 65 K), because of inaccuracies in the PES around the Van der Waals complexes that become important at low temperatures. The unimolecular reaction rate is namely calculated as the decay of the Van der Waals encouter or pre-reactive complex. The activation energies including ZPE correction and starting from a pre-reactive minimum for the reactions CH_4 + OH, CD_4 + OH and CH_4 + OD are 2575, 2915, and 2605 K (21.1, 24.2, and 21.7 kJ/mol), respectively.

The unimolecular reaction rate is of interest for surface reactivity, since most interstellar-relevant reactions will take place between two reactants that have adsorbed on a grain prior to the reaction. Such reactants are thermalized and can only react after finding each other. As long as they are close together, they may attempt to react several times. In Fig. 7, the corresponding calculated rate constants are depicted. In general, rate constant values decrease with temperature. The exact values are given in Table 3, while Table 4 lists the parameters fitted to Eqn. 1. A

kinetic isotope effect k_{CH_4+OD}/k_{CD_4+OH} of approximately ten is obtained between 200 and 65 K. Therefore, a similar value for the KIE at even lower temperatures seems to be a reasonable estimation. This is consistent with the conclusion derived in the previous paragraph for the experiments; the reaction CH_4 + OD is found to take place whereas for CD_4 + OH no reaction products are found, that is, the first reaction is definitely faster than the second.

4. Astrophysical Implications

For the calculation of the reaction rate constants, we have focused here on the reaction between OH radicals and CH_4 molecules because it provides a simple system that can be potentially extended to other H-abstraction reactions involving OH radicals and larger hydrocarbons as was proposed by Garrod (2013) and Acharyya et al. (2015). As mentioned before, OH radicals are present in the H_2O -rich layers of the ice as a result of non-energetic hydrogenation reactions and weak FUV irradiation that photodissociates water. Therefore, it is expected that they are available for reactions (Garrod 2013). The abundances of solid CH_4 can reach levels of several percent with respect to water ice in a variety of environments, such as, low- and high-mass young stellar objects, quiescent clouds, cold cores, and cometary ices (Öberg et al. 2008; Boogert et al. 2015; Le Roy et al. 2015 and references therein). Moreover, methane is mostly formed in a water-rich environment (Boogert et al. 2015). Therefore, the reaction CH_4 + OH is likely to occur in space at low temperatures. An important product of the aforementioned H-abstraction reaction is the methyl radical. In the ISM, solid CH_3 is an intermediate reaction product in the formation of methane. It can also be formed through UV-, electrons- and ions-induced dissociation reactions from ice mixtures containing methane (Milligan & Jacox 1967; Bohn et al. 1994; Palumbo et al. 2004; Hodyss et al. 2011; Kim & Kaiser 2012; Wu et al. 2012, 2013; Materese et al. 2014, 2015; Lo et al. 2015; J.B. Bossa 2015; Chin et al. 2016). The solid CH_4 + OH abstraction reaction investigated here, however, can be an important channel for the formation of methyl radicals under interstellar analog conditions. It allows CH_3 production without the need for photodissociation and strong energetic processing of the ice.

Recent disk and protostellar models showed that several molecules with a methyl group ($R-CH_3$) are present in ices (Vasyunin & Herbst 2013; Furuya & Aikawa 2014; Walsh et al. 2014; Taquet et al. 2015; Drozdovskaya et al. 2016). Moreover, one of the outcomes of the Rosetta mission is the discovery of heavy organic matter on the comet 67P/Churyumov-Gerasimenko (Goesmann et al. 2015; Fray et al. 2016). Also in this case, several species contain a methyl group. Therefore, surface reactions involving the CH_3 functional group are assumed to play an important role in enhancing the molecular complexity in space. Large hydrocarbon radicals can be created by the H-abstraction from any larger molecule of the form $R-CH_3$, which is then available for subsequent reactions.

The fits to Eqn. 1 can be used by the astrochemical modeling community as an initial approach to describing H-abstraction reactions from methane in the solid phase via the Langmuir-Hinshelwood mechanism. These fits are definitely valid down to temperatures of 65 K and we can recommend extrapolation down to ~35 K. Although the desorption temperature of pure methane is relatively low, when it is trapped in the water ices, it is expected to desorb only when water does, that is, around 100 K (Collings et al. 2004). In order to assure a smooth implementation of such rate constants in models, it is crucial to realize that the expressions typically used in rate equation models to describe tunneling involve the rectangular barrier approximation. Then, reaction rates are proportional to a probability $P = \exp(\frac{2a}{\hbar}\sqrt{2\mu E})$. With a typical barrier width a of 1 Å, the activation energies mentioned above, and masses μ of 1 or 2 amu depending on H- or D-abstraction, as well as the ratio between the probabilities, P_{CH_4+OD} and P_{CD_4+OH}, and thus between the rates, would be approximately 5×10^3. Here, we show with the use of instanton calculations, that the KIE is approximately ten at low temperature, which is orders of magnitude lower than the value generally used in rate equation models. This implies that current models may need to improve on their implementation of H- vs. D-abstraction reactions. Although here we show the effect for one reaction only, this conclusion also holds for other astrochemically relevant reactions, such as $H + H_2O_2 \longrightarrow H_2O + OH$ (Lamberts et al. 2016b).

Table 3. Unimolecular reaction rate constants.

	CH_4 + OH T_C = 323.5 K	CD_4 + OH T_C = 240.2 K	CH_4 + OD T_C = 323.1 K
T (K)	k (s^{-1})	k (s^{-1})	k (s^{-1})
300	2.18×10^9		2.19×10^9
240	2.97×10^8		2.73×10^8
230		3.26×10^7	1.78×10^8
220		1.90×10^7	1.20×10^8
200	6.10×10^7	5.93×10^6	5.07×10^7
190		3.19×10^6	3.32×10^7
180		1.67×10^6	2.25×10^7
170		8.57×10^5	
160		4.32×10^5	
150		2.17×10^5	
140	2.53×10^6		1.64×10^6
130	1.01×10^6	6.36×10^4	5.83×10^5
120	4.14×10^5		2.22×10^5
110	1.82×10^5	1.12×10^4	8.07×10^4
100	6.94×10^4	2.81×10^3	2.96×10^4
95	4.94×10^4	1.51×10^3	1.75×10^4
90	3.22×10^4	8.37×10^2	1.03×10^4
85	2.06×10^4	4.74×10^2	6.01×10^3
80	1.34×10^4	2.73×10^2	3.51×10^3
75	8.91×10^3	1.63×10^2	1.99×10^3
70	5.86×10^3	9.93×10^1	1.11×10^3
65	3.88×10^3	6.29×10^1	6.08×10^2

Table 4. Parameters fitted down to 65 K to describe the abstraction reactions CH_4 + OH, CD_4 + OH, and CH_4 + OD, respectively.

Parameter	CH_4 + OH	CD_4 + OH	CH_4 + OD
α (s^{-1})	1.24×10^{11}	5.86×10^{10}	1.45×10^{11}
β	1	1	1
γ (K)	1201	1468	1252
T_0 (K)	83.1	85.0	73.9

5. Conclusions

With this combined laboratory-theoretical study, we provide a proof-of-principle for the importance of incorporating tunneling in the description of OH-mediated hydrogen abstraction. First, through solid phase experiments, we find that the surface reac-

tion CH_4 + OD indeed proceeds faster than CD_4 + OH at 15 K as expected for tunneled reactions. Second, instanton calculations of unimolecular rate constants quantify the processes and give a kinetic isotope effect of approximately ten at 65 K. Such unimolecular rate constants relate to the thermalized Langmuir-Hinshelwood process, the main mechanism used to explain the non-energetic surface formation of species on and in interstellar ices. For the first time, rate constants at temperatures down to 65 K for the CH_4 + OH reaction are provided with accompanying fits to allow easy implementation into astrochemical models. The calculated rate constants also show that the rectangular barrier approximation currently used in models inaccurately estimates kinetic isotope effects for the title reaction by approximately two orders of magnitude.

Acknowledgements. We kindly thank Jun Li and Hua Guo for providing the potential energy surface. Astrochemistry in Leiden in general was supported by the European Community's Seventh Framework Programme (FP7/2007–2013) under grant agreement no. 238258, the Netherlands Research School for Astronomy (NOVA) and from the Netherlands Organization for Scientific Research (NWO) within the framework of the Dutch Astrochemistry Network. SI acknowledges the Royal Society for financial support. TL was supported by the Dutch Astrochemistry Network financed by NWO. TL and JK were financially supported by the European Union's Horizon 2020 research and innovation programme (grant agreement No. 646717, TUNNELCHEM).

References

Acharyya, K., Herbst, E., Caravan, R. L., et al. 2015, Mol. Phys., 113, 2243

Aguilera-Iparraguirre, J., Curran, H. J., Klopper, W., & Simmie, J. M. 2008, J. Phys. Chem. A, 112, 7047

Allen, J. W., Green, W. H., Li, Y., Guo, H., & Suleimanov, Y. V. 2013, J. Chem. Phys., 138

Arasa, C., van Hemert, M. C., van Dishoeck, E. F., & Kroes, G. J. 2013, J. Phys. Chem. A, 117, 7064

Atkinson, R. 2003, Atmos. Chem. Phys., 3, 2233

Bockelée-Morvan, D., Crovisier, J., Erard, S., et al. 2016, MNRAS, DOI 10.1093/mnras/stw2428

Bohn, R. B., Sandford, S. A., Allamandola, L. J., & Cruikshank, D. P. 1994, Icarus, 111, 151

Boogert, A. C. A., Gerakines, P. A., & Whittet, D. C. B. 2015, ARA&A, 53, 541

Boogert, A. C. A., Helmich, F. P., van Dishoeck, E. F., et al. 1998, A&A, 336, 352

Callan, C. G. & Coleman, S. 1977, Phys. Rev. D, 16, 1762

Caravan, R. L., Shannon, R. J., Lewis, T., Blitz, M. A., & Heard, D. E. 2015, J. Phys. Chem. A, 119, 7130

Chang, Q. & Herbst, E. 2014, ApJ, 787, 135

Chin, C.-H., Chen, S.-C., Liu, M.-C., Huang, T.-P., & Wu, Y.-J. 2016, ApJS, 224, 17

Chuang, K.-J., Fedoseev, G., Ioppolo, S., van Dishoeck, E., & Linnartz, H. 2016, 455, 1702

Collings, M. P., Anderson, M. A., Chen, R., et al. 2004, 354, 1133

Corchado, J. C., Bravo, J. L., & Espinosa-Garcia, J. 2009, The Journal of Chemical Physics, 130

Cuppen, H. M., Ioppolo, S., Romanzin, C., & Linnartz, H. 2010, Phys. Chem. Chem. Phys., 12, 12077

Drozdovskaya, M. N., Walsh, C., van Dishoeck, E. F., et al. 2016, 462, 977

Edling, J. A., Richardson, H. H., & Ewing, G. E. 1987, J. Mol. Struct., 157, 167

Espinosa-García, J., Nyman, G., & Corchado, J. C. 2009, The Journal of Chemical Physics, 130

Fernández-Ramos, A., Ellingson, B. A., Meana-Pañeda, R., Marques, J. M. C., & Truhlar, D. G. 2007, Theor. Chem. Acc., 118, 813

Fray, N., Bardyn, A., Cottin, H., et al. 2016, Nature, advance online publication

Fu, B., Kamarchik, E., & Bowman, J. M. 2010, The Journal of Chemical Physics, 133

Furuya, K. & Aikawa, Y. 2014, ApJ, 790, 97

Garrod, R. T. 2013, ApJ, 765, 60

Gierczak, T., Talukdar, R. K., Herndon, S. C., Vaghjiani, G. L., & Ravishankara, A. R. 1997, J. Phys. Chem. A, 101, 3125

Giguère, P. A. & Srinivasan, T. 1975, Chem. Phys. Lett., 33, 479

Goesmann, F., Rosenbauer, H., Bredehöft, J. H., et al. 2015, Science, 349

Goumans, T. P. M. & Kästner, J. 2011, J. Phys. Chem. A, 115, 10767

Graff, M. M. & Wagner, A. F. 1990, The Journal of Chemical Physics, 92

Hasegawa, T. I., Herbst, E., & Leung, C. M. 1992, Astrophys. J. Suppl. Ser., 82, 167

Hodyss, R., Howard, H. R., Johnson, P. V., Goguen, J. D., & Kanik, I. 2011, Icarus, 214, 748

Hodyss, R., Johnson, P. V., Stern, J. V., Goguen, J. D., & Kanik, I. 2009, Icar., 200, 338

Ioppolo, I., Fedoseev, G., Lamberts, T., Romanzin, C., & Linnartz, H. 2013, Rev. Sci. Instrum. , 84, 073112

Ioppolo, S., Cuppen, H. M., Romanzin, C., van Dishoeck, E. F., & Linnartz, H. 2008, ApJ, 686, 1474

Ioppolo, S., Cuppen, H. M., Romanzin, C., van Dishoeck, E. F., & Linnartz, H. 2010, Phys. Chem. Chem. Phys., 12, 12065

J.B. Bossa, D.M. Paardekooper, K. I. H. L. 2015, 17, 17346

Kästner, J. 2014, WIREs Comput. Mol. Sci., 4, 158

Kästner, J., Carr, J. M., Keal, T. W., et al. 2009, J. Phys. Chem.A, 113, 11856

Kim, Y. S. & Kaiser, R. I. 2012, ApJ, 758, 37

Lacy, J. H., Carr, J. S., Evans, II, N. J., et al. 1991, ApJ, 376, 556

Lamberts, T., Cuppen, H. M., Ioppolo, I., & Linnartz, H. 2013, Phys. Chem. Chem. Phys., 15, 8287

Lamberts, T., de Vries, X., & Cuppen, H. M. 2014, Faraday Discuss., 168, 327

Lamberts, T., Fedoseev, G., Puletti, F., et al. 2016a, MNRAS, 455, 634

Lamberts, T., Samanta, P. K., Köhn, A., & Kästner, J. 2016b, Phys. Chem. Chem. Phys., DOI: 10.1039/C6CP06457D

Le Roy, L., Altwegg, K., Balsiger, H., et al. 2015, A&A, 583, A1

Li, J. & Guo, H. 2015, J. Chem. Phys., 143

Li, Y., Suleimanov, Y. V., Li, J., Green, W. H., & Guo, H. 2013, The Journal of Chemical Physics, 138

Lo, J.-I., Chou, S.-L., Peng, Y.-C., et al. 2015, ApJS, 221, 20

Materese, C. K., Cruikshank, D. P., Sandford, S. A., Imanaka, H., & Nuevo, M. 2015, ApJ, 812, 150

Materese, C. K., Cruikshank, D. P., Sandford, S. A., et al. 2014, ApJ, 788, 111

Meisner, J., Rommel, J. B., & Kästner, J. 2011, J. Comput. Chem., 32, 3456

Metz, S., Kästner, J., Sokol, A. A., Keal, T. W., & Sherwood, P. 2014, WIREs Comput. Mol. Sci., 4, 101

Meyer, J. & Reuter, K. 2014, Angew. Chem. Int. Ed., 53, 4721

Miller, W. H. 1975, J. Chem. Phys., 62

Milligan, D. E. & Jacox, M. E. 1967, The Journal of Chemical Physics, 47

Momose, T., Hoshina, H., Fushitani, M., & Katsuki, H. 2004, Vibr. Spec., 34, 95

Noble, J. A., Dulieu, F., Congiu, E., & Fraser, H. J. 2011, The Astrophysical Journal, 735, 121

Nyman, G., van Harrevelt, R., & Manthe, U. 2007, J. Phys. Chem. A, 111, 10331

Oba, Y., Osaka, K., Watanabe, N., Chigai, T., & Kouchi, A. 2014, Faraday Discuss. , 168, 185

Oba, Y., Watanabe, N., Hama, T., et al. 2012, ApJ, 749, 67

Oba, Y., Watanabe, N., Kouchi, A., Hama, T., & Pirronello, V. 2010, ApJ, 712, L174

Öberg, K. I. 2016, Chem. Rev.

Öberg, K. I., Boogert, A. C. A., Pontoppidan, K. M., et al. 2008, The Astrophysical Journal, 678, 1032

Palumbo, M. E., Ferini, G., & Baratta, G. A. 2004, Advances in Space Research, 33, 49

Richardson, J. O. 2016, J. Chem. Phys., 144, 114106

Rommel, J. B., Goumans, T. P. M., & Kästner, J. 2011, J. Chem. Theory Comput., 7, 690

Shannon, R., Blitz, M., Goddard, A., & Heard, D. 2013, Nat. Chem., 5, 745

Taquet, V., López-Sepulcre, A., Ceccarelli, C., et al. 2015, ApJ, 804, 81

Tschersich, K. G. 2000, Journal of Applied Physics, 87

Tschersich, K. G. & von Bonin, V. 1998, J. Appl. Phys., 84

van Dishoeck, E. F., Herbst, E., & Neufeld, D. A. 2013, Chemical Reviews, 113, 9043

Vasyunin, A. I. & Herbst, E. 2013, ApJ, 762, 86

Wada, A., Mochizuki, N., & Hiraoka, K. 2006, ApJ, 644, 300

Walsh, C., Millar, T. J., Nomura, H., et al. 2014, A&A, 563, A33

Wang, W. & Zhao, Y. 2012, J. Chem. Phys., 137

Weber, A. S., Hodyss, R., Johnson, P. V., Willacy, K., & Kanik, I. 2009, ApJ, 703, 1030

Werner, H.-J., Knowles, P. J., Knizia, G., et al. 2015, MOLPRO, version 2015.1, a package of ab initio programs, see http://www.molpro.net

Wu, Y.-J., Chen, H.-F., Chuang, S.-J., & Huang, T.-P. 2013, ApJ, 768, 83

Wu, Y.-J., Wu, C. Y. R., Chou, S.-L., et al. 2012, ApJ, 746, 175

Zheng, J. & Truhlar, D. G. 2010, Phys. Chem. Chem. Phys., 12, 7782

Zins, E.-L., Pirim, C., Joshi, P. R., & Krim, L. 2012, J. Phys. Chem. A, 116, 12357

Appendix A: Gas-phase bimolecular reaction rate constants

In the gas phase, rotational motion is not restricted, and moreover the symmetry of the reactant and transition states needs to be taken into account in the calculation of the rate constants (Fernández-Ramos et al. 2007). The symmetry factor used here is 12, resulting from the pointgroups T_d for the methane molecule, $C_{\infty V}$ for OH, and C_s for the eclipsed and staggered instanton configurations. Furthermore, here, bimolecular rate constants are applicable that include the chance of meeting, hence the different units compared to unimolecular rate constants.

Table A.1 shows the calculated bimolecular reaction rate constants in the range 300–70 K. The highest temperatures calculated here can be compared to the values at the lower end of the range recommended by Atkinson (2003), or, more specifically, to the gas-phase experimental data points around 200 K provided by Gierczak et al. (1997). We choose the lowest temperature possible, since the influence of tunneling will then be more prominent. This shows that the maximum deviation between our instanton rate constants and their experiments is one order of magnitude.

This overestimation has two origins, firstly the harmonic approximation in instanton theory is known to lead to an overestimation of the rate constants at temperatures close to the crossover temperature (Goumans & Kästner 2011). At the low temperatures that we are interested in for surface reactivity, however, the harmonic approximation is valid and the part of the overestimation that stems from this thus vanishes. Furthermore, the lower barrier on the PES with respect to CCSD(T)-F12 calculations (see Section 2.2) leads to a small overestimation of the rate constant as well.

The ratio between H- and D-abstraction by the OH radical, k_{CH_4+OH}/k_{CD_4+OH}, is the same for our calculations and for the gas-phase experimental values (Gierczak et al. 1997), namely ∼12.5. Additionally, the ratio k_{CH_4+OH}/k_{CH_4+OD} is also similar, ∼0.73 in both cases. These ratios are calculated in the range where the calculations overlap with the gas-phase experiments,that is, around 230 K. This agreement with bimolecular gas-phase experimental data provides a good basis for quantifying unimolecular surface processes.

Table A.1. Bimolecular reaction rate constants.

	CH_4 + OH	CD_4 + OH	CH_4 + OD
	T_C = 323.5 K	T_C = 240.2 K	T_C = 323.1 K
T	k	k	k
(K)	(s^{-1})	(s^{-1})	(s^{-1})
300	1.35×10^{-13}		1.78×10^{-13}
240	1.80×10^{-14}		2.54×10^{-14}
230		1.14×10^{-15}	
220		6.46×10^{-16}	1.22×10^{-14}
200	3.92×10^{-15}	1.91×10^{-16}	5.89×10^{-15}
190		1.00×10^{-16}	4.20×10^{-15}
180		5.15×10^{-17}	3.14×10^{-15}
170		2.60×10^{-17}	
160		1.30×10^{-17}	
150		6.48×10^{-18}	
140	2.37×10^{-16}		4.23×10^{-16}
130	1.07×10^{-16}	1.94×10^{-18}	1.90×10^{-16}
120	5.16×10^{-17}		9.61×10^{-17}
110	2.64×10^{-17}	3.72×10^{-19}	4.96×10^{-17}
100	1.36×10^{-17}	1.00×10^{-19}	2.80×10^{-17}
95		5.68×10^{-20}	2.14×10^{-17}
90	8.68×10^{-18}	3.33×10^{-20}	1.68×10^{-17}
85	6.74×10^{-18}	2.02×10^{-20}	1.36×10^{-17}
80		1.27×10^{-20}	
75		8.36×10^{-21}	
70		5.72×10^{-21}	